



# A Complete Single Asperity-Based Statistical Gaussian Rough Surface Contact Model

A. Megalingam<sup>1</sup> · K. S. Hanumanth Ramji<sup>2</sup>

Received: 22 April 2020 / Revised: 22 July 2020 / Accepted: 22 September 2020 / Published online: 6 October 2020  
© Springer Nature Switzerland AG 2020

## Abstract

Understanding the corrosion behavior of rough surface contacts needs the contact interaction of rough surfaces at asperity level. Generally, single asperity-based statistical rough surface contact model is predominating one in exploring contact behavior of rough surfaces. The FEM-based single asperity contact model is being used extensively to explain the elastic, elastic–plastic, and fully plastic behavior of the rough surface contacts. The empirical expressions to calculate the exact transitions (elastic to elastic–plastic and elastic–plastic to fully plastic states) are still incomplete. The earlier FEM-based single asperity contact models didn't give mathematical expressions to exactly calculate the elastic, elastic–plastic, and fully plastic transition states by accounting the combined effect of material properties. In this way, in the present work, empirical expressions are developed to calculate the exact transitions of elastic, elastic–plastic and fully plastic states by accounting the combined effect of Young's modulus, material yield strength, and Poisson's ratio. The empirical expressions to calculate the dimensionless contact load and contact area are developed for elastic, elastic–plastic, and fully plastic states in terms of dimensionless interference,  $E/Y$  ratio, and Poisson's ratio. Further, it is observed that the plasticity index is not a complete parameter to explore the contact behavior of rough surface contacts. In high surface plasticity index case, the material properties influence significantly compared to the low surface plasticity index case. The Poisson's ratio significantly influences in low  $E/Y$  ratio materials in all the surface plasticity index cases.

**Keywords** Contact analysis · Single asperity · Finite element analysis · Material properties

## List of Symbols

$A_n$	Nominal contact area
$A$	Real contact area
$A^*$	Dimensionless real contact area, $A_r/A_n$
$d$	Separation based on asperity heights
$d^*$	Dimensionless separation, $d/\sigma$
$E$	Hertz elastic modulus
$E'$	Reduced elastic modulus
$H$	Hardness of softer material
$h$	Separation based on surface heights
$h^*$	Dimensionless separation $h/\sigma$
$N$	Total number of asperities
$P$	Contact load
$P^*$	Dimensionless contact load, $P/A_n E'$

$R$	Asperity radius of curvature
$Y$	Yield strength of asperity
$y_s^*$	$H^* - d^*$
$z$	Height of an asperity measured from the mean of asperity heights
$z^*$	Dimensionless height of an asperity
$\beta$	Surface roughness parameter, $\eta\beta\sigma$
$\Phi^*$	Dimensionless distribution function of asperity heights
$\eta$	Area density of asperity
$\nu$	Poisson's ratio
$\sigma$	Standard deviation of surface heights
$\sigma_s$	Standard deviation of asperity heights
$\sigma_y$	Yield strength of asperity
$\omega^*$	Dimensionless interference, $\omega/\sigma$
$\omega_c$	Critical interference at the inception of plastic deformation
$\omega_c^*$	Dimensionless critical interference, $\omega_c/\sigma$
$\psi$	Plastic index

✉ A. Megalingam  
mechmega@gmail.com

<sup>1</sup> Department of Mechanical Engineering, Bannari Amman Institute of Technology, Sathyamangalam, Erode, Tamil Nadu, India

<sup>2</sup> Department of Mechatronics, Bannari Amman Institute of Technology, Sathyamangalam, Erode, Tamil Nadu, India

## Subscripts

c	Critical values at yielding inception
EPS	Elastic–Plastic Start

EPE Elastic–Plastic End  
FPS FullyPlastic Start

## 1 Introduction

Study of tribological systems in the applications of bearings, clutches, brakes, mechanical seals, cams, gears, electrical contacts, mechanical joints, biomedical components, and mechanical interfaces under corrosive environment is important one. Tribocorrosion explains the material degradation process due to mechanical sliding and electrochemical processes. Understanding the fundamental of material degradation process in tribocorrosion systems at microscopic level is an involved task. When two solid bodies come into contact due to surface irregularities, the contact occurs at discrete spots called as asperities. The asperities may deform elastically, elastoplastically, or plastically which lead to mechanical wear and wear accelerated corrosion. Stachowiak et al. [1], numerically simulated to predict tribocorrosion of passive metals. They represented the asperities as cuboids positioned at different heights. They used the passivation model to predict the corrosion wear and hard pin slides on metal asperities to calculate the mechanical wear. Cao et al. [2–4] developed a tribocorrosion model for passive metals by accounting plastic deformation of asperities and combined the mechanical wear, chemical wear and hydrodynamic lubrication to quantify the material damage. Guadalupe et al. [5] attempted the applicability of existing tribocorrosion model that include the mechanical, chemical, and lubrication concepts with three different CoCr inhomogeneous alloys. Dalmau et al. [6] applied boundary element method to simulate the contact surface deformation for the mechanical wear calculation based on Archard wear law and galvanic coupling model [7] to calculate chemical wear in order to evaluate the material degradation with time to predict the tribocorrosion. Ghanbarzadeh et al. [8, 9] numerically and experimentally studied the synergistic effects of corrosion wear and asperity-based mechanical wear through established electrochemistry model and Archard's mechanical model. Knowing the deformation behavior of contacting asperities in rough surface contact interaction will enhance the understanding tribocorrosion phenomenon. Contact interaction of rough surfaces is analyzed through statistical approach, deterministic approach, fractal approach, and experiments. In this way, several statistical rough surface contact models have been proposed. A pioneer contact model is the Greenwood and Williamson [10] elastic contact model. Abbott and Firestone [11] developed a fully plastic contact known as surface micro geometry model. Chang et al. (CEB model) [12] bridged the fully elastic and

fully plastic contact approaches by an elastic–plastic contact model on the basis of volume of conservation of plastically deformed asperities. This model adopted an abrupt transition from fully elastic to fully plastic state. The results showed that the mean separation is large and real area of contact is small in elastic–plastic contact than elastic contact for the same plasticity index and contact load. Zhao et al. (ZMC model) [13] devised an elastic–plastic contact model, which interpolates the fully elastic to fully plastic states. This model used mathematical functions to smoothen the fully elastic, elasticplastic, and fully plastic states. Smaller mean separation and larger real area of contact were predicted by the ZMC model than the GW model at any given plasticity index and contact load. ZMC model showed a complete elastic–plastic contact phenomenon between rough surfaces for wide range of plasticity index and contact load compared to GW model and CEB model. The exact inception of elastic–plastic to fully plastic was not governed. Kogut and Etsion (KE Model) [14, 15] developed a FEM-based elastic–plastic single asperity-based rough surface contact model. This model developed generic empirical relationship for dimensionless mean contact pressure, dimensionless contact load, and the dimensionless contact area with the dimensionless interference ratio. The results showed that the fully plastic deformation on the contact surface occurs at a constant dimensionless interference ratio of 110, at that stage the mean contact pressure ratio ( $P_{\text{mean}}/Y$ ) reaches 2.8. They incorporate the single asperity finite element results to predict the contact parameters of rough surfaces, i.e., the mean separation, contact load, and the real area of contact in dimensionless forms. For calculating the contact parameters, they used the same hardness value throughout the statistical model, but they varied the standard deviation of surface heights and the plasticity index from 0.5 to 8, as in the CEB model. Their results were identical with CEB model till the plasticity index of 0.6 as pure elastic. The plasticity index of 1.4 marked as the transition of elastic to elastic–plastic and above the plasticity value of 8 entered to fully plastic. Jackson and Green [16, 17] (JG model) extended the Kogut and Etsion work to account the geometry and material effects in the analysis. For calculating the critical interference, this model used von Mises yield criterion and material yield strength directly. This model formulated new empirical relationships to calculate contact load and contact area with respect to the deformation for elastic–perfectly plastic case based on the FEM results. The results showed that the mean contact pressure ( $p/Y$ ) ratio does not reach 2.8 for most of the yield strength values. The end of the elastic–plastic state is not identified. Further the empirical expressions are not updated for the general elastic–plastic cases. The developed empirical relations of dimensionless contact parameters

are used to study the rough surface contact. In which, the plasticity index was varied from 0.5 to 100 by varying the material properties alone. They concluded that till the plasticity index of 10, the KE model and their model can be interchangeable but for high plasticity index values, large differences are observed.

Brizmer et al. [18, 19] (BKE model) conducted FEM-based single asperity contact model under perfect slip and full stick conditions till the dimensionless interference ratio of 110. This model considered the materials with  $E/Y$  greater than 500 and  $E_t/E$  of 0.02 with Poisson's ratio of 0.25, 0.35, and 0.45. The results showed the contact parameters are insensitive to contact conditions (perfect slip or full stick), independent of  $E/Y$ ,  $E_t/E$ , asperity radius but slightly depend on Poisson's ratio. This model didn't consider the high yield materials and the effect of tangent modulus. Shankar and Mayuram [20, 21] (SM model) extended the JG model to study the formation of elastic core, the transition of elastic-plastic to fully plastic state and the effect of tangent modulus. The results showed that the elastic core formation, the maximum  $P_{\text{mean}}/Y$  ratio and the transition from elastic-plastic to fully plastic state depend on  $E/Y$  and  $E_t/E$  ratios. The effect of Poisson's ratio is not considered. Megalingam and Mayuram [22] (MM model) found exact inceptions of elastic-plastic and fully plastic contacts then, formulated complex empirical relations for contact parameters but didn't extend to study the contact of rough surfaces. Wang and Wang [23] developed a continuously differentiable cubic polynomial function based cubic elastic plastic single asperity contact model (Cubic model) which greatly reduced the error of Wang's [24] compact and continuous model but didn't extend to study the effect of plasticity index. Recently, Peng et al. [25] initially studied the contact behavior of a single asperity with deformable substrate using finite element method and extended to study the elastic-plastic contact behavior of statistical rough surface contacts. Ghaednia et al. [26, 27] studied the contact behavior of a deformable sphere against a deformable flat for elastic perfectly plastic materials and strain hardening materials but didn't cover wide range of materials.

From the foregoing literature survey, it is observed that the exact transition of contact state is not completely explained. Apart from other single asperity contact models, MM model explored the influence of Young's modulus, yield strength, and Poisson's ratio on the transition states (elastic, elastic-plastic, and fully plastic) but didn't calculate the interference ratios of elastic, elastic-plastic, and fully plastic transition states and also didn't extend to study the statistical contact behavior of rough surfaces. In this way, the present work attempts to calculate the exact transition of contact states and to study the contact behavior of Gaussian

rough surface by accounting the combined effect of Poisson's ratio,  $E/Y$  ratio, and surface roughness.

## 2 Single Asperity Contact Model

In statistical rough surface contact model, a single asperity contact model is initially developed and then it is extended to the whole rough surface. In this way, in the present work, a deformable spherical asperity contact against rigid flat plane is modeled and analyzed using ANSYS package. Due to axi-symmetric nature of spherical asperity, a quarter of a circle is considered as the asperity and it is allowed to contact against a rigid line acts as rigid flat plane. The model is discretized with 1,04,176 eight node solid elements (PLANE 82) in which 80% of elements are occupied near the contact zone which is shown in Fig. 1. The surface-to-surface contact elements, CONTAC 172 and TARGE 169, are used to define the contact interaction with perfect slip condition. The material properties, Young's modulus of 200 GPa, Poisson's ratios of 0.25, 0.35, and 0.45, and yield strength ranging from 210 to 2520 MPa are considered [22, 28]. The rigid flat plane is constrained to move in all direction. The vertical side of the hemispherical asperity is assigned as axi-symmetric one whereas the top side is given vertical displacement to interfere with the rigid flat plane as shown in Fig. 1. The contact load and contact length are extracted from the nodal results. The meshed model is verified with Hertz elastic solution and the mesh density is doubled in order to achieve less than 1% deviation in contact parameters results between the iterations under elastic-perfectly plastic condition.

In the present work, the critical interference, critical contact load and critical contact area of asperity are considered from the BKE model. The empirical relations [Eqs. (2) and (3)] are developed to calculate the exact elastic, elastic-plastic, and fully plastic contact states' interference ratios from the results of FEM model. Figure 2 shows the elastic, elastic-plastic, and fully plastic contact zones and their boundary which is affected by  $E/Y$  ratio and Poisson's ratio significantly. The incompressibility phenomenon is sustained till the asperity reaches the elastic-plastic contact state limit but beyond this limit, the above phenomenon decreases and the high Poisson's ratio material attains the fully plastic contact state quickly. Such a behavior is observed for wide range of  $E/Y$  ratio materials with certain significant deviations. The deviation among the Poisson's ratio cases is small at elastic-plastic contact state for all  $E/Y$  ratios but beyond the elastic-plastic limit the deviation among the Poisson's ratio cases decreases as the yield strength decreases.

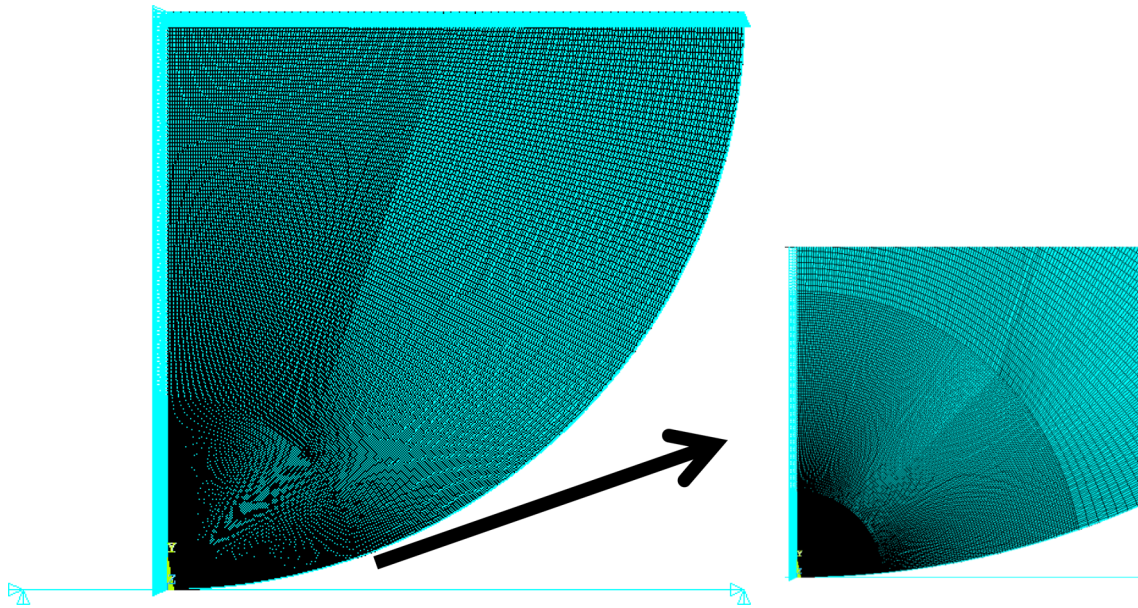
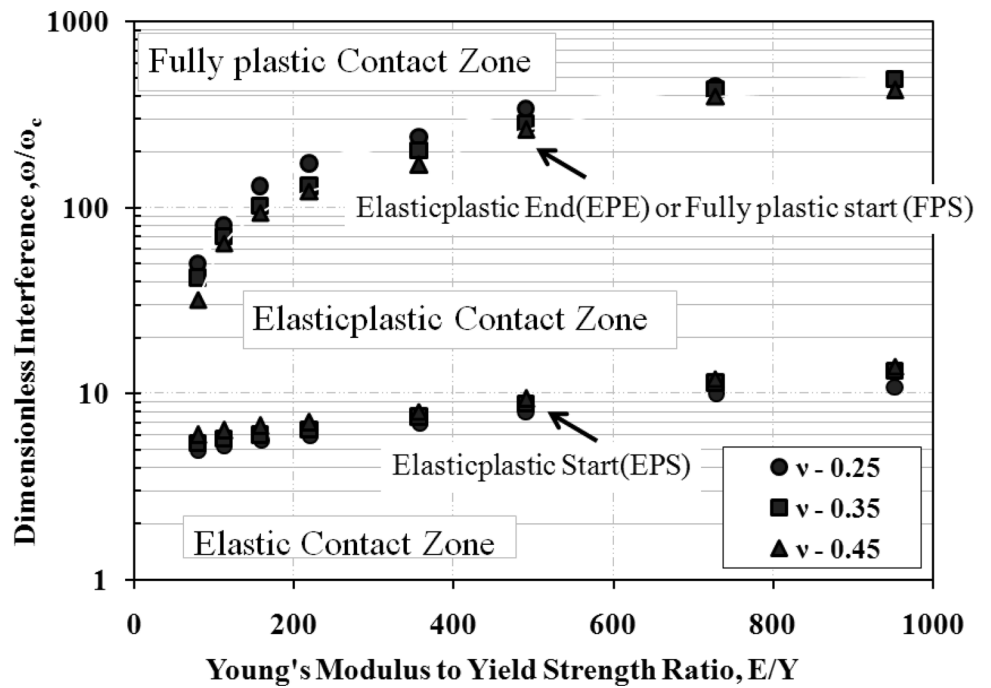


Fig. 1 Finite element model of single asperity in contact with a rigid flat plane

Fig. 2 Elastic, elastic–plastic, and fully plastic contact zones with their boundary



$$\omega_c = \left( C_v \frac{\pi(1 - \nu^2)Y}{2E^*} \right)^2 R, \quad \text{where } C = 1.234 + 1.256\nu \quad 1 \leq \frac{\omega}{\omega_c} \leq \left( \frac{\omega}{\omega_c} \right)_{\text{EPS}} \tag{1}$$

$$P_c = \frac{4E^* \sqrt{R}}{3} \omega_c^{3/2} \quad A_c = \pi R \omega_c$$

$$\begin{aligned} \frac{P}{P_c} = & -0.63035699 + 1.6509794 \frac{\omega}{\omega_c} - 0.0054352502 \left( \frac{E}{Y} \nu \right) \\ & + 0.1257165 \left( \frac{\omega}{\omega_c} \right)^2 + 2.5256505 \times 10^{-5} \left( \frac{E}{Y} \nu \right)^2 \\ & - 0.0016703999 \left( \frac{\omega}{\omega_c} \right) \left( \frac{E}{Y} \nu \right) - 0.0024036996 \left( \frac{\omega}{\omega_c} \right)^3 \\ & - 3.5243671 \times 10^{-8} \left( \frac{E}{Y} \nu \right)^3 + 1.3968421 \times 10^{-6} \left( \frac{\omega}{\omega_c} \right) \\ & \left( \frac{E}{Y} \nu \right)^2 + 2.1352305 \times 10^{-5} \left( \frac{\omega}{\omega_c} \right)^2 \left( \frac{E}{Y} \nu \right) \end{aligned} \tag{4}$$

Elastic to Elasticplastic contact transition interference ratio  $\left( \frac{\omega}{\omega_c} \right)_{\text{EPS}}$  :

$$\begin{aligned} \left( \frac{\omega}{\omega_c} \right)_{\text{EPS}} = & -28.685653 + 14.311243 \ln \left( \frac{E}{Y} \right) + 143.68877\nu \\ & - 2.8398888 \left( \ln \left( \frac{E}{Y} \right) \right)^2 - 492.76268\nu^2 + 6.0956348\nu \\ & \left( \ln \left( \frac{E}{Y} \right) \right) + 0.23181555 \left( \ln \left( \frac{E}{Y} \right) \right)^3 + 251.75487\nu^3 \\ & + 33.424224\nu^2 \left( \ln \left( \frac{E}{Y} \right) \right) - 2.2544612\nu \left( \ln \left( \frac{E}{Y} \right) \right)^2 \end{aligned} \tag{2}$$

Elasticplastic to fully plastic contact transition interference ratio  $\left( \frac{\omega}{\omega_c} \right)_{\text{EPE}}$  or  $\left( \frac{\omega}{\omega_c} \right)_{\text{FPS}}$  :

$$\left( \frac{\omega}{\omega_c} \right)_{\text{EPE}} = \left( \frac{\omega}{\omega_c} \right)_{\text{FPS}} = \left( \frac{-418.99543 + 238.9742 \ln \left( \frac{E}{Y} \right) - 44.322073 \left( \ln \left( \frac{E}{Y} \right) \right)^2 + 2.7023394 \left( \ln \left( \frac{E}{Y} \right) \right)^3 + 3.6246545 \ln(\nu) + 3.0238763 \left( \ln \left( \frac{E}{Y} \right) \right)^2}{1 - 0.30906927 \ln \left( \frac{E}{Y} \right) + 0.02429745 \left( \ln \left( \frac{E}{Y} \right) \right)^2 + 0.021323967 \ln(\nu) + 0.01169986 \ln(\nu)^2} \right) \tag{3}$$

The empirical relations of Eqs. (4) to (13) are developed from FEM results using MATLAB curve fitting technique to calculate dimensionless contact load and dimensionless contact area in elastic, elastic-plastic, and fully plastic contact zones which are

Elasticplastic contact and fully plastic contact  $\frac{\omega}{\omega_c} \geq \left( \frac{\omega}{\omega_c} \right)_{\text{EPS}}$

Contact Load Calculation:  $79.36 \leq (E/Y) \leq 219.418$

$$\left( \frac{\omega}{\omega_c} \right)_{10} \leq \frac{\omega}{\omega_c} \leq \left( \frac{\omega}{\omega_c} \right)_{100}$$

Elastic contact  $\frac{\omega}{\omega_c} \leq 1 \quad P = \frac{4E^2 \sqrt{R}}{3} \omega^{3/2}$

$$\begin{aligned} \frac{P}{P_c} = & -19.629104 + 3.1676153 \frac{\omega}{\omega_c} + \frac{1872.2509}{\left( \frac{E}{Y} \nu \right)} + 0.02235644 \left( \frac{\omega}{\omega_c} \right)^2 - \frac{88057.918}{\left( \frac{E}{Y} \nu \right)^2} + \frac{5.8057865}{\left( \frac{E}{Y} \nu \right)} \left( \frac{\omega}{\omega_c} \right) \\ & - 7.7680827 \times 10^{-5} \left( \frac{\omega}{\omega_c} \right)^3 + \frac{1046233.2}{\left( \frac{E}{Y} \nu \right)^3} + \frac{218.7350}{\left( \frac{E}{Y} \nu \right)^2} \left( \frac{\omega}{\omega_c} \right) - \frac{0.30734565}{\left( \frac{E}{Y} \nu \right)} \left( \frac{\omega}{\omega_c} \right)^2 \end{aligned} \tag{5}$$

$$\left(\frac{\omega}{\omega_c}\right)_{100} \leq \frac{\omega}{\omega_c} \leq \left(\frac{\omega}{\omega_c}\right)_{350}$$

$$\begin{aligned} \frac{P}{P_c} = & 4183.044 - \frac{1,097,906.5}{\frac{\omega}{\omega_c}} - \frac{58,194.196}{\left(\frac{E}{Y}\nu\right)} + \frac{1.1263213 \times 10^8}{\left(\frac{\omega}{\omega_c}\right)^2} - \frac{431,206.08}{\left(\frac{E}{Y}\nu\right)^2} + \frac{15,800,081}{\left(\frac{\omega}{\omega_c}\right)\left(\frac{E}{Y}\nu\right)} \\ & - \frac{4.0769242 \times 10^9}{\left(\frac{\omega}{\omega_c}\right)^3} + \frac{9,851,981.8}{\left(\frac{E}{Y}\nu\right)^3} - \frac{38,095,542}{\left(\frac{\omega}{\omega_c}\right)^2\left(\frac{E}{Y}\nu\right)^2} - \frac{8.745662 \times 10^8}{\left(\frac{\omega}{\omega_c}\right)^2\left(\frac{E}{Y}\nu\right)} \end{aligned} \tag{6}$$

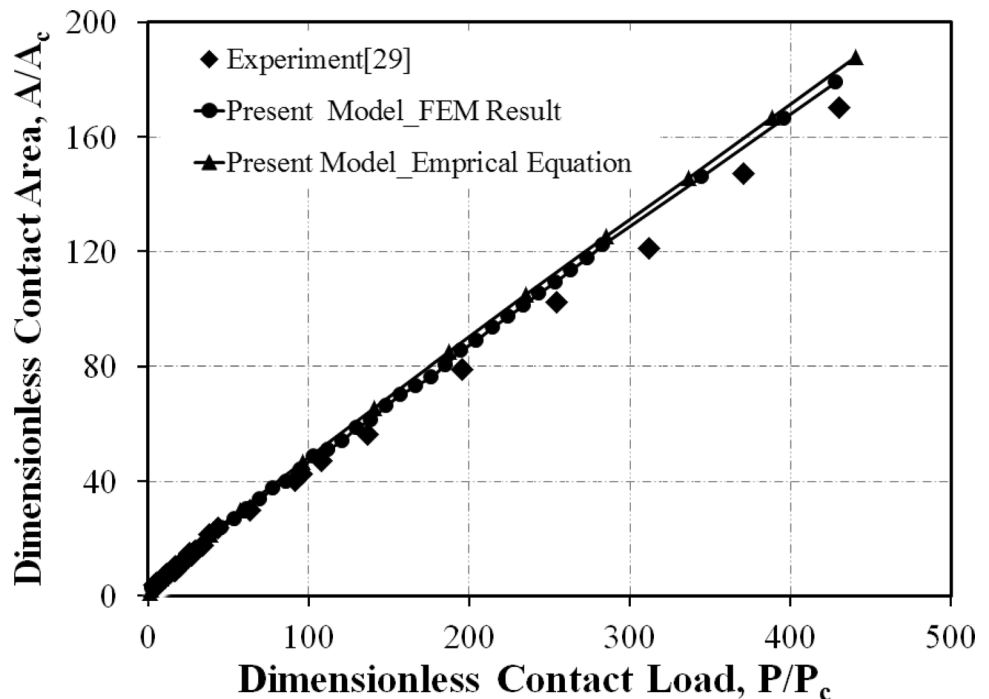
$$\left(\frac{\omega}{\omega_c}\right)_{350} \leq \frac{\omega}{\omega_c} \leq \left(\frac{\omega}{\omega_c}\right)_{500}$$

$$\begin{aligned} \frac{P}{P_c} = & 2979.2477 - 9.2112948 \frac{\omega}{\omega_c} - 1737.5584 \log\left(\frac{E}{Y}\nu\right) - 0.0096166147 \left(\frac{\omega}{\omega_c}\right)^2 + 323.2957 \left[\log\left(\frac{E}{Y}\nu\right)\right]^2 \\ & + 6.0053902 \left(\frac{\omega}{\omega_c}\right) \log\left(\frac{E}{Y}\nu\right) + 1.2597004 \times 10^{-6} \left(\frac{\omega}{\omega_c}\right)^3 - 19.995791 \left[\log\left(\frac{E}{Y}\nu\right)\right]^3 \\ & - 0.5987779 \left(\frac{\omega}{\omega_c}\right) \left[\log\left(\frac{E}{Y}\nu\right)\right]^2 + 0.0016820239 \left(\frac{\omega}{\omega_c}\right)^2 \log\left(\frac{E}{Y}\nu\right) \end{aligned} \tag{7}$$

Contact area calculation:  $79.36 \leq (E/Y) \leq 219.418$

Elastic contact  $\frac{\omega}{\omega_c} \leq 1 \quad A = \pi R \omega$

Fig. 3 Validation of the present model



$$1 \leq \frac{\omega}{\omega_c} \leq \left(\frac{\omega}{\omega_c}\right)_{\text{EPS}} \quad 79.36 \leq (E/Y) \leq 952.38$$

$$\left(\frac{A}{A_c}\right) = \frac{1}{\left[-2.7700138 - 0.98294541 \frac{\ln\left(\frac{w}{w_c}\right)}{\left(\frac{w}{w_c}\right)} + \frac{0.9575097}{\left(\frac{w}{w_c}\right)} - 0.025575525 \left(\frac{E\nu}{Y}\right)^{0.5} \ln\left(\frac{E\nu}{Y}\right) - 0.14589492 \left(\ln\left(\frac{E\nu}{Y}\right)\right)^2 + 0.30367008 \left(\frac{E\nu}{Y}\right)^{0.5} + 0.82909436 \ln\left(\frac{E\nu}{Y}\right) - \frac{1.0616582}{\ln\left(\frac{E\nu}{Y}\right)} + \frac{4.180017}{\left(\frac{E\nu}{Y}\right)^{0.5}}\right]} \quad (8)$$

### Elastic-plastic contact

$$\left(\frac{\omega}{\omega_c}\right)_{\text{EPS}} \leq \frac{\omega}{\omega_c} \leq \left(\frac{\omega}{\omega_c}\right)_{\text{EPE}} \quad 79.36 \leq (E/Y) \leq 112.00 \text{ and } \left(\frac{\omega}{\omega_c}\right)_{\text{EPS}} \leq \frac{\omega}{\omega_c} \leq 80 \quad 112 \leq (E/Y) \leq 952.38$$

$$\left(\frac{A}{A_c}\right) = \frac{1}{\left[0.00019606755 + \frac{0.40342394}{\left(\frac{w}{w_c}\right)} + \frac{1.2779085}{\left(\frac{w}{w_c}\right)^{1.5}} - 0.43040423 \frac{\ln\left(\frac{E\nu}{Y}\right)}{\left(\frac{E\nu}{Y}\right)} + \frac{3.474929}{\left(\frac{E\nu}{Y}\right)} - \frac{27.89297}{\left(\frac{E\nu}{Y}\right)^{1.5}} + 29.078631 \frac{\ln\left(\frac{E\nu}{Y}\right)}{\left(\frac{E\nu}{Y}\right)^2} - \frac{6.5915847}{\left(\frac{E\nu}{Y}\right)^2} + 539141.72e^{-\left(\frac{E\nu}{Y}\right)}\right]} \quad (9)$$

$$112 \leq (E/Y) \leq 356.63 \quad 80 \leq \frac{\omega}{\omega_c} \leq \left(\frac{\omega}{\omega_c}\right)_{\text{EPE}}$$

$$\left(\frac{A}{A_c}\right) = e^{\left[-13.099.513 + 0.05157601 \left(\frac{w}{w_c}\right)^{0.5} - \frac{19.277949}{\ln\left(\frac{w}{w_c}\right)} + \frac{131.390.44}{\ln\left(\frac{E\nu}{Y}\right)} - \frac{245.877.04}{\left(\frac{E\nu}{Y}\right)^{0.5}} + 406536.42 \frac{\ln\left(\frac{E\nu}{Y}\right)}{\left(\frac{E\nu}{Y}\right)} - \frac{1171565.6}{\left(\frac{E\nu}{Y}\right)} + \frac{2.320.145.3}{\left(\frac{E\nu}{Y}\right)^{1.5}} - \frac{1.610.606.4}{\left(\frac{E\nu}{Y}\right)^2}\right]} \quad (10)$$

$$356.63 \leq (E/Y) \leq 952.38$$

$$80 \leq \frac{\omega}{\omega_c} \leq \left(\frac{\omega}{\omega_c}\right)_{\text{EPE}}$$

$$\left(\frac{A}{A_c}\right) = \frac{1}{\left[-0.066643587 + \frac{0.40466773}{\left(\frac{w}{w_c}\right)} + \frac{1.3112678}{\left(\frac{w}{w_c}\right)^{1.5}} + \frac{8.0533218}{\left(\frac{E\nu}{Y}\right)^{0.5}} - 99.171604 \frac{\ln\left(\frac{E\nu}{Y}\right)}{\left(\frac{E\nu}{Y}\right)} + \frac{570.45608}{\left(\frac{E\nu}{Y}\right)} - \frac{2799.4925}{\left(\frac{E\nu}{Y}\right)^{1.5}} + 1792.1313 \frac{\ln\left(\frac{E\nu}{Y}\right)}{\left(\frac{E\nu}{Y}\right)^2} + \frac{979.26285}{\left(\frac{E\nu}{Y}\right)^2}\right]} \quad (11)$$

### For fully plastic contact

$$\frac{\omega}{\omega_c} \geq \left(\frac{\omega}{\omega_c}\right)_{\text{FPS}} \quad 79.36 \leq (E/Y) \leq 356.63$$

$$\left(\frac{A}{A_c}\right) = e^{\left[-13099.513 + 0.05157601 \left(\frac{w}{w_c}\right)^{0.5} - \frac{19.277949}{\ln\left(\frac{w}{w_c}\right)} + \frac{131390.44}{\ln\left(\frac{E\nu}{Y}\right)} - \frac{245877.04}{\left(\frac{E\nu}{Y}\right)^{0.5}} + 406536.42 \frac{\ln\left(\frac{E\nu}{Y}\right)}{\left(\frac{E\nu}{Y}\right)} - \frac{1171565.6}{\left(\frac{E\nu}{Y}\right)} + \frac{2320145.3}{\left(\frac{E\nu}{Y}\right)^{1.5}} - \frac{1610606.4}{\left(\frac{E\nu}{Y}\right)^2}\right]} \quad (12)$$

$$356.63 \leq (E/Y) \leq 952.38$$



$$\left(\frac{A}{A_c}\right) = \frac{1}{\left[-0.066643587 + \frac{0.40466773}{\left(\frac{w}{w_c}\right)} + \frac{1.3112678}{\left(\frac{w}{w_c}\right)^{1.5}} + \frac{8.0533218}{\left(\frac{E\nu}{Y}\right)^{0.5}} - 99.171604 \frac{\ln\left(\frac{E\nu}{Y}\right)}{\left(\frac{E\nu}{Y}\right)} + \frac{570.45608}{\left(\frac{E\nu}{Y}\right)} - \frac{2799.4925}{\left(\frac{E\nu}{Y}\right)^{1.5}} + 1792.1313 \frac{\ln\left(\frac{E\nu}{Y}\right)}{\left(\frac{E\nu}{Y}\right)^2} + \frac{979.26285}{\left(\frac{E\nu}{Y}\right)^2}\right]} \quad (13)$$

### 3 Validation of Present Model

In order to validate the present work, the material properties,  $E = 1.39 \times 10^5 \text{ N/mm}^2$ ,  $\nu = 0.33$ , and  $\sigma_y = 345 \text{ N/mm}^2$  are considered from the experimental work of Ovcharenko et al. [29] and are applied in the present FEM model and the developed empirical relations. The results are shown in Fig. 3 as the variation of dimensionless contact area with dimensionless contact load. The present FEM results show good agreement with experimental result [29]. Additionally, the contact load and contact area are calculated using the developed equations for the same material properties which are shown in Fig. 3. The results of developed equations show good agreement with FEM results and experimental results.

### 4 Statistical Rough Surface Contact Model

In statistical rough surface contact model, the asperities are of same size and shape. The heights of the asperities are normally assumed to follow Gaussian distribution. If the asperities are assumed to spherical in nature, then they have same radius of curvature and are not interacting themselves as shown in Fig. 4.

Based on single asperity contact model results and Greenwood and Williamson model assumptions, contact parameters like total contact area and total contact load with mean separation are calculated with the following steps:

Some base parameters that should be considered between contacting rough surfaces. Mainly two reference planes can be defined. (i.e., mean of asperity heights and mean of the surface heights). Let  $z$  and  $d$  are the asperity heights and separation of the surfaces with  $R$  is the radius of the asperity.  $h$  is the separation of the surfaces from the reference planes.

All the models utilized Gaussian distribution for the asperity height distribution and that is given as

$$\phi^*(z^*) = \frac{1}{\sqrt{2\pi}} \frac{\sigma}{\sigma_s} \exp\left[-0.5\left(\frac{\sigma}{\sigma_s}\right)^2 (z^*)^2\right]$$

The standard deviation  $\sigma_s$  and  $\sigma$  correspond to the asperity and surface heights, respectively, and are related by [30]:

$$\sigma^2 = \sigma_s^2 + \frac{3.717 \times 10^{-4}}{\eta^2 R^2}$$

All the dimensions are normalized by  $\sigma$  and the dimensionless values are denoted by \*.

Critical interference can be normalized with  $\sigma$  to give:

$$\omega_c^* = \frac{\omega_c}{\sigma}$$

$y_s^*$  is the difference between  $h^*$  and  $d^*$  and is calculated by

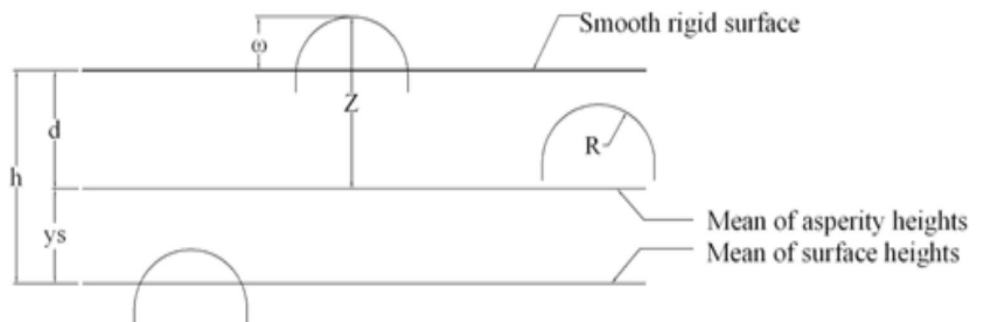
$$y_s^* = h^* - d^* = \frac{1.5}{\sqrt{108\pi}\beta}$$

The number of asperities on the contacting surface can be found by multiplying the nominal surface by the area density of the asperities:

$$N = \eta A_n$$

Then, the total number of asperities in contact is defined as follows:

Fig. 4 Statistical rough surface contact model





$$N_c = \eta A_n \int_d^\infty \phi(z) dz$$

The individual asperity contact area,  $A$ , and force,  $P$ , are functions of each asperity's interference,  $\omega$ . Thus, the contribution of all asperities of a height  $z$  to the total contact area and total contact force can be calculated as:

$$A(z) = \eta A_n A(z - d) \phi(z)$$

$$P(z) = \eta A_n P(z - d) \phi(z)$$

Then, the total area of contact and total contact force between the surfaces is found by simply integrating the above equation over the entire range of asperity contact:

$$A(d) = \eta A_n \int_d^\infty A(z - d) \phi(z) dz$$

$$P(d) = \eta A_n \int_d^\infty P(z - d) \phi(z) dz$$

Greenwood and Williamson [1] defines plasticity index to relate the critical interference and the roughness of the surface to the plastic deformation of the surface and the relation is

$$\psi = \sqrt{\frac{\sigma_s}{\omega_c}}$$

The plasticity index also relates the critical interference and the roughness of the surface to the plastic deformation of the surface. Here, the surface roughness as well as the material properties is also varied.

### 5 Result and Discussion

In order to assess the present empirical relation-based rough surface contact model, the Zhao et al. model [13] material properties  $E_1 = E_2 = 207$  GPa,  $\nu_1 = \nu_2 = 0.29$  and  $\sigma_y = 700$  MPa and surface parameters as given Table 1 are considered.

The fraction of total real area of contact in apparent area of contact as a function of dimensionless mean separation

**Table 1** Surface parameters and plasticity index values [13]

$\sigma/R$	$\beta$	$\psi$
$8.75 \times 10^{-5}$	0.0302	0.5
$3.02 \times 10^{-4}$	0.0414	1.0
$1.77 \times 10^{-3}$	0.0601	2.5

for different plasticity index is shown in Fig. 5a–c. For the plasticity index case of 0.5 (Fig. 5a), the maximum dimensionless contact area deviation is 3%, 5.5%, and 5.5% for Cubic model, BKE model, and JG model, respectively, with the present model due to more number of elastically deforming asperities. For the plasticity index case of 1.0 (Fig. 5b), the maximum dimensionless contact area deviation is 4%, 6.7%, and 7.5% for Cubic model, BKE model, and JG model, respectively, with the present model due to large number of elastic deformation of asperities, few elastic–plastically deforming asperities, and the difference in the formulation of elastic–plastic contact area calculation in each model. For the plasticity index case of 2.5 (Fig. 5c), the maximum dimensionless contact area deviation is 3.3%, 4.6%, and 5.7% for Cubic model, BKE model, and JG model, respectively, with the present model due to more number of elastic–plastic deformation of asperities and the difference in the formulation of elastic–plastic contact area and fully plastic contact area calculations in each model. The present model dimensionless contact area shows good agreement with the other models in all the plasticity index cases.

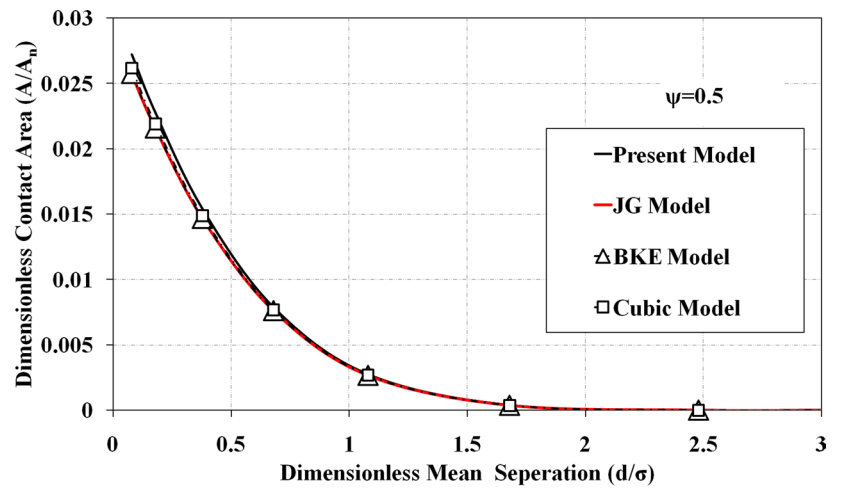
The dimensionless contact load against the dimensionless mean separation is provided for all plasticity index cases in Fig. 6a–c. In  $\psi = 0.5$  case (Fig. 6a), the maximum dimensionless contact load deviation is 4%, 5.0% and 4.8% for Cubic model, BKE model and JG model, respectively, with the present model at  $d/\sigma$  of 0.08. In the case of  $\psi = 1.0$  (Fig. 6b), the maximum dimensionless contact load deviation is 5.4% at  $d/\sigma$  of 0.08 with the present model but the BKE model and JG model showed 4.0% and 3.0%, respectively, with the present model at  $d/\sigma$  of 3.0. In the case of  $\psi = 2.5$  (Fig. 6c), the maximum dimensionless contact load deviation is 10.8%, 4.9%, and 4.6% for Cubic model, BKE model, and JG model, respectively, with the present model at  $d/\sigma$  of 0.08 due to different formulation of contact load calculation and the cut off elastic–plastic contact state differs in each model.

The dimensionless contact area against the dimensionless contact load for different plasticity index is shown in Fig. 7a–c. The present model shows larger bearing area support for the same dimensionless contact load compared to other models due to the appropriate prediction of elastic–plastic behavior. In the case of  $\psi = 1.0$ , the present model and cubic model behave similarly whereas the JG model and BKE model underestimate. In the case of  $\psi = 2.5$ , the cubic model overestimates compared to other models due to its mathematical formulation. In general, the present model shows good agreement with other models in low and high plasticity cases.

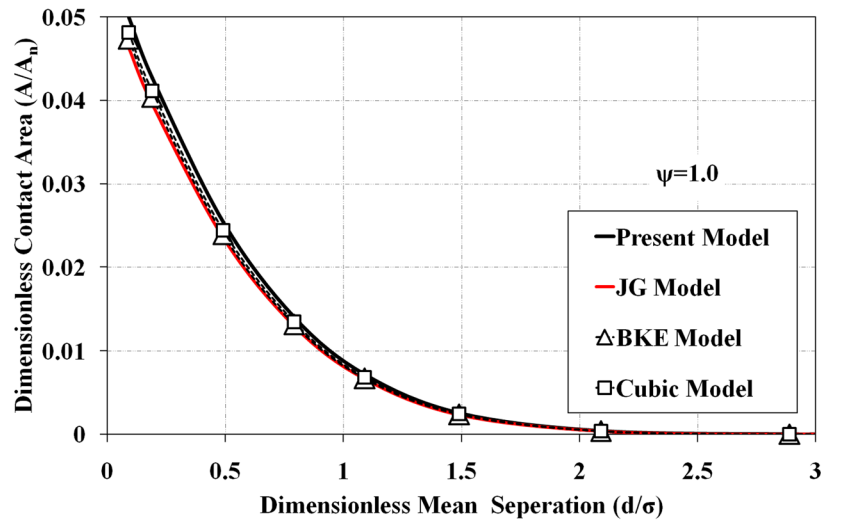
#### 5.1 Effect of $E/Y$ Ratio and Poisson's Ratio

In order to explore the effect of  $E/Y$  ratio and Poisson's ratio on rough surface contacts parameters, two extreme

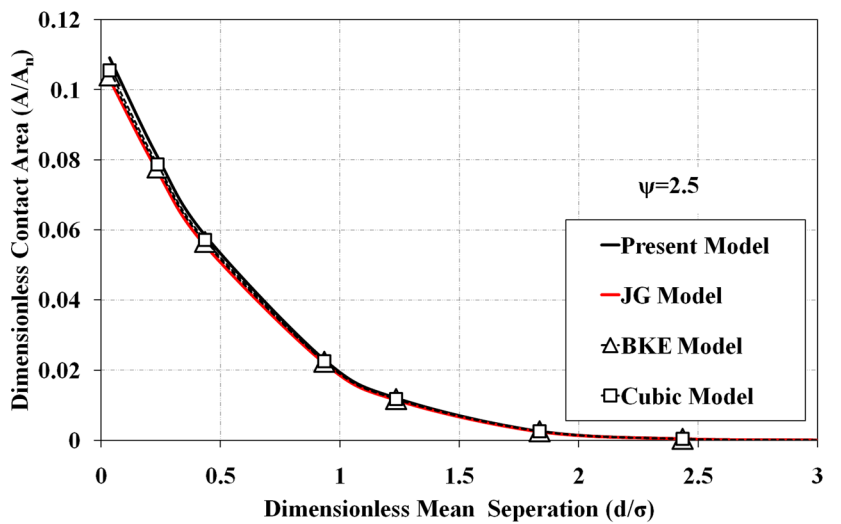
**Fig. 5** **a** Variation of dimensionless real area of contact with dimensionless mean separation for plasticity index  $\psi=0.5$ . **b** Variation of dimensionless real area of contact with dimensionless mean separation for plasticity index  $\psi=1.0$ . **c** Variation of dimensionless real area of contact with dimensionless mean separation for plasticity index  $\psi=2.5$



(a)

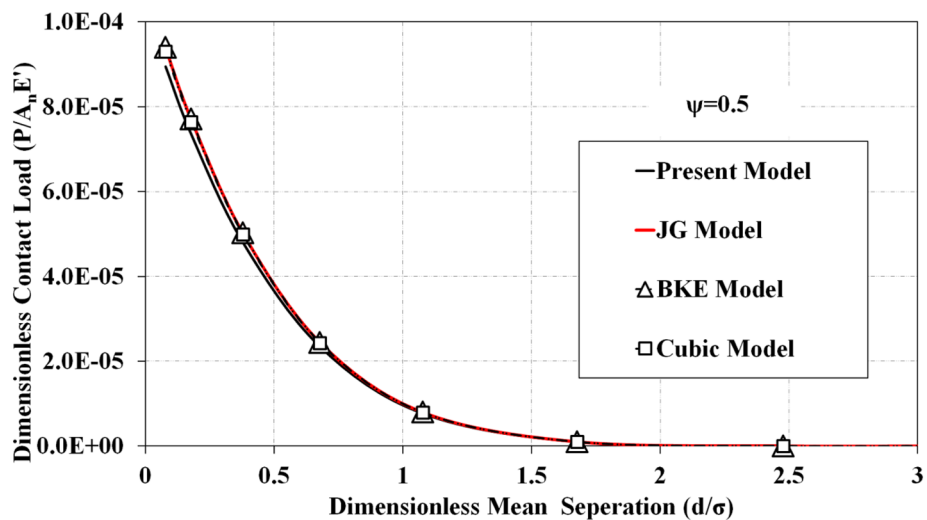


(b)

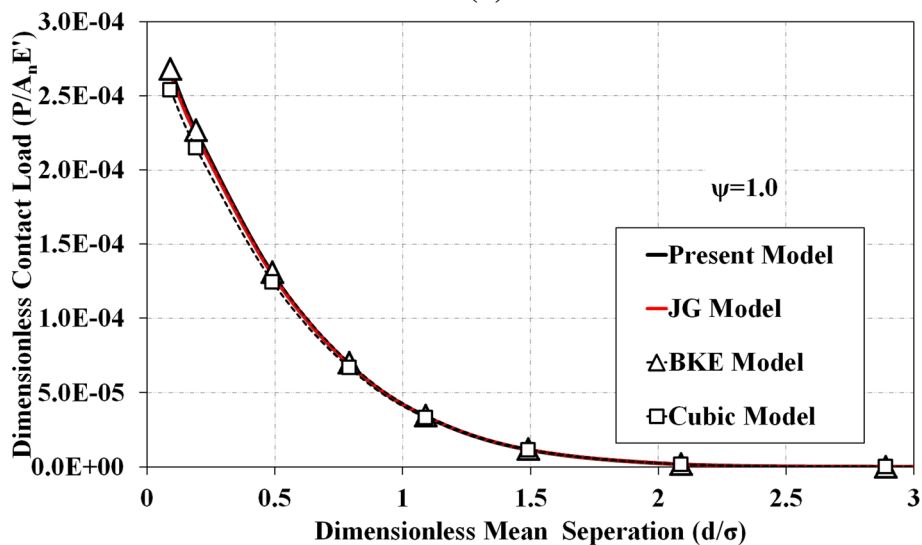


(c)

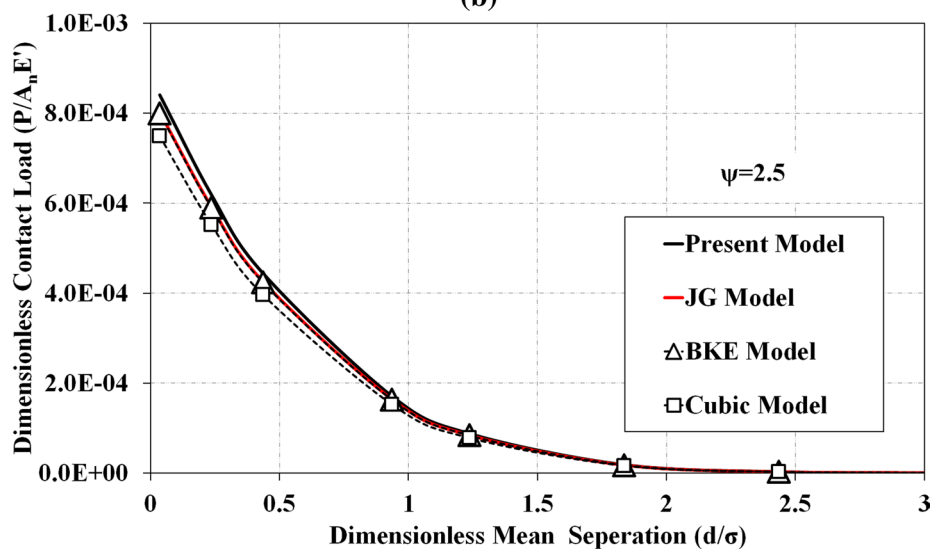
**Fig. 6** **a** Variation of dimensionless contact load with dimensionless mean separation for plasticity index  $\psi=0.5$ . **b** Variation of dimensionless contact load with dimensionless mean separation for plasticity index  $\psi=1.0$ . **c** Variation of dimensionless contact load with dimensionless mean separation for plasticity index  $\psi=2.5$



(a)

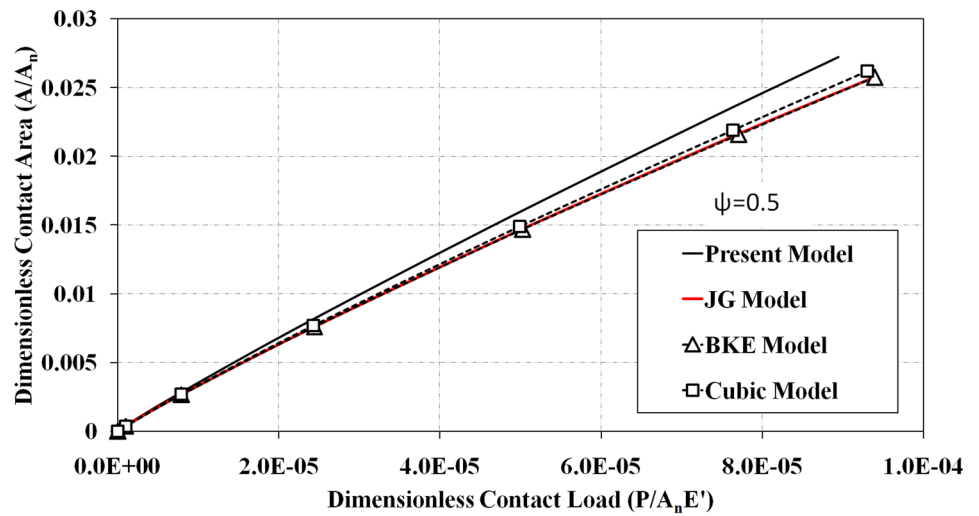


(b)

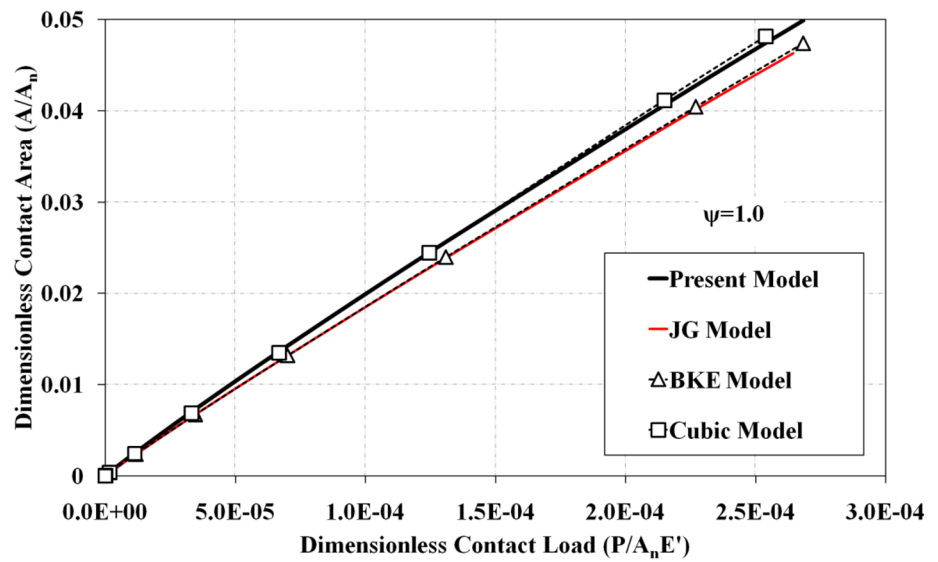


(c)

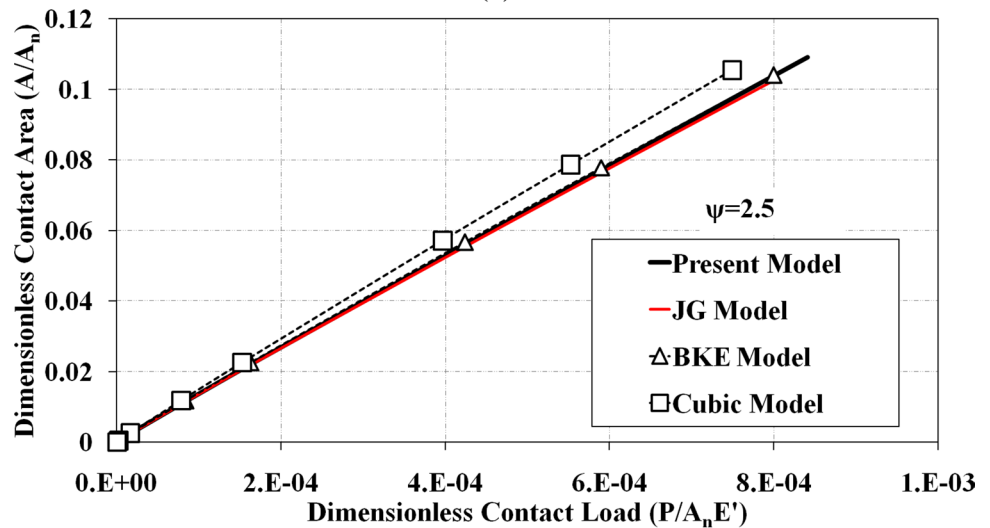
**Fig. 7** **a** Variation of dimensionless real area of contact with dimensionless contact load for plasticity index  $\psi=0.5$ . **b** Variation of dimensionless real area of contact with dimensionless contact load for plasticity index  $\psi=1.0$ . **c** Variation of dimensionless real area of contact with dimensionless contact load for plasticity index  $\psi=2.5$



(a)

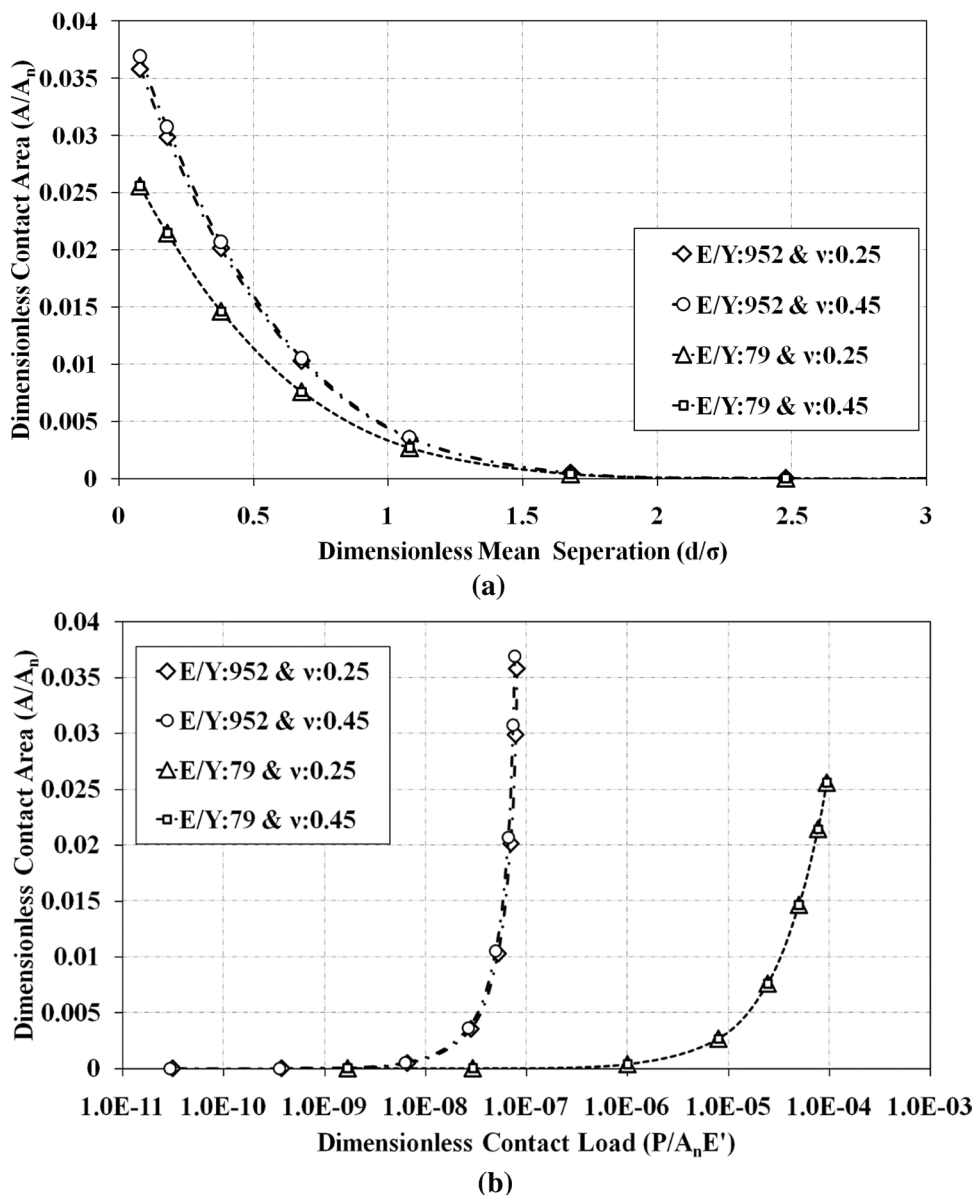


(b)



(c)

**Fig. 8 a** Variation of dimensionless contact area with dimensionless mean separation for plasticity index of 0.5. **b** Variation of dimensionless contact area with dimensionless contact load for plasticity index of 0.5

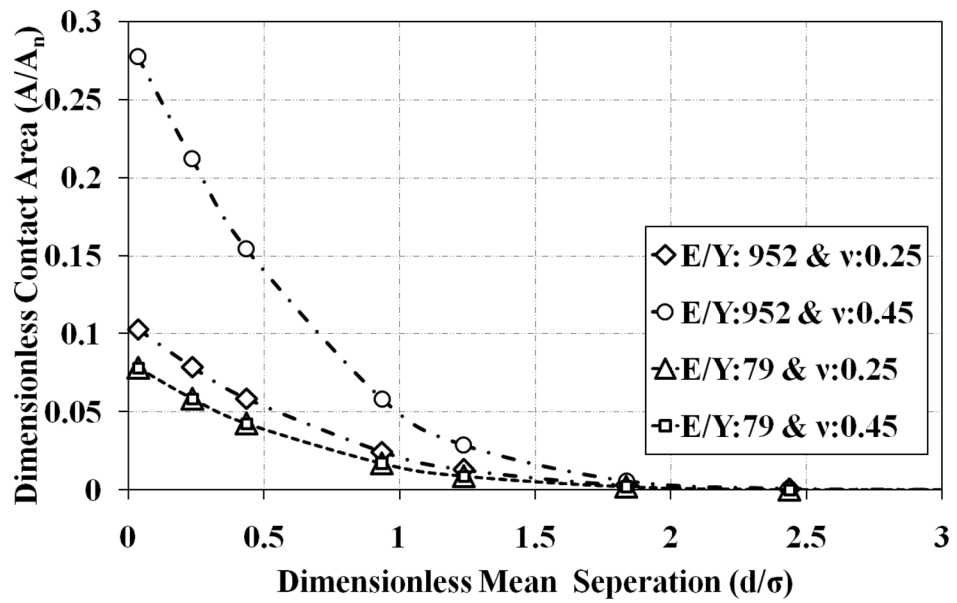


cases of  $E=200$  GPa,  $\nu=0.25$  and  $0.45$ ,  $\sigma_y=210$  MPa, and  $2520$  MPa are considered from [22]. Figure 8a shows the variation of dimensionless real area of contact as a function of dimensionless mean separation for plasticity index of 0.5. The effect of Poisson’s ratio on contact area is insignificant for low and high strength materials but the low strength material marks larger bearing area support compared to high strength material due to large number of elastically deformed asperities. Figure 8b shows the variation of dimensionless real area of contact as a function of dimensionless contact load for plasticity index of 0.5. As like contact area, the effect of Poisson’s ratio on contact load is insignificant for low and high strength materials but the high strength material shows increased contact load than the low strength material. For the difference of 91% yield strength, three order

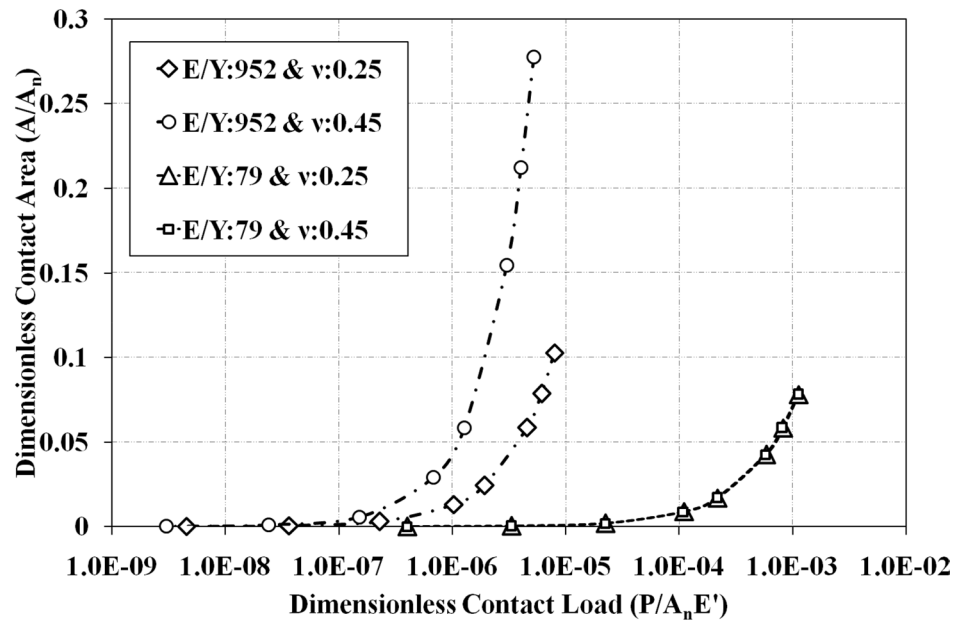
increased bearing load support is provided by high strength material.

Figure 9a shows the variation of dimensionless real area of contact as a function of dimensionless mean separation for plasticity index of 2.5. The effect of Poisson’s ratio on contact area is insignificant for high strength material. In low strength and high Poisson’s ratio material case, the incompressibility phenomena decrease due to elastic–plastic and fully plastic deformation of asperities so larger bearing area support is achieved for the same interference. Figure 9b shows the variation of dimensionless real area of contact as a function of dimensionless contact load for plasticity index of 2.5. As like contact area, the effect of Poisson’s ratio on contact load is insignificant for high strength material. In low strength material case, low Poisson’s ratio material shows increased contact

**Fig. 9 a** Variation of dimensionless contact area with dimensionless mean separation for plasticity index of 2.5. **b** Variation of dimensionless contact area with dimensionless contact load for plasticity index of 2.5



(a)



(b)

load than the high Poisson’s ratio material due to lack of incompressibility phenomena after the inception of yielding. For the difference of 91% yield strength, two order increased bearing load support is provided by low strength material.

### 6 Conclusion

- Empirical relations are developed to calculate exact transition interference of elastic, elastic–plastic, and fully plastic contact states in terms of  $E/Y$  ratio and Poisson’s ratio.

- Empirical relations are developed to calculate elastic, elasticplastic, and plastic states dimensionless contact load and contact area in terms of interference ratio,  $E/Y$  ratio, and Poisson’s ratio.
- The developed statistical Gaussian rough surface contact model shows good agreement with BKE model compared to JG and Cubic models in low to high plasticity index cases.
- In low plasticity index case: for 12 times increased  $E/Y$  ratio, the dimensionless contact area is increased 0.7 times than low  $E/Y$  ratio of 79 whereas dimensionless contact load is increased three order in low  $E/Y$  ratio

for the same dimensionless contact area but the effect of Poisson’s ratio is negligible due to large number of elastically deformed asperities.

- In high plasticity index case: in low Poisson’s ratio case, for 12 times increased  $E/Y$  ratio, only 0.3 times increased dimensionless contact area is attained whereas the high Poisson’s ratio achieved two order increased dimensionless contact area due to large number of elastic–plastically deformed asperities.
- In high plasticity index case: for 12 times increased  $E/Y$  ratio, two (low Poisson’s ratio) to three (high Poisson’s ratio) order increased dimensionless contact load is attained for same dimensionless contact area.
- In high plasticity index case: the effect of Poisson’s ratio is negligible in the low  $E/Y$  ratio case but in 12 times increased  $E/Y$  ratio case, the low Poisson’s ratio case marked maximum of 0.6 times increased dimensionless contact load compared to high Poisson’s ratio due to large elastic–plastic and plastic deformation of asperities and the difference exists in incompressibility nature.

### Compliance with Ethical Standards

**Conflict of interest** On behalf of all authors, the corresponding author states that there is no conflict of interest.

### Appendix

Previous Elastic–Plastic Contact Models

*Jackson and Green Model (JG model)*

$$\omega_c = \left( \frac{\pi CS_y}{2E^*} \right)^2 R, \quad \text{where } C = 1.295 \exp(0.736\nu)$$

$$P_c = \frac{4}{3} \left( \frac{R}{E^*} \right)^2 \left( \frac{C}{2} \pi S_y \right)^3 \quad A_c = \pi^3 \left( \frac{CS_y R}{2E^*} \right)^2$$

For  $\omega/\omega_c \geq 1.9$ ,

$$A_{JG} = \pi R \omega \left( \frac{\omega}{1.9\omega_c} \right)^B$$

$$P_{JG} = P_c \left\{ \left[ \exp \left( -\frac{1}{4} \left( \frac{\omega}{\omega_c} \right)^{5/12} \right) \right] \left( \frac{\omega}{\omega_c} \right)^{3/2} + \frac{4H_G}{CS_y} \left[ 1 - \exp \left( -\frac{1}{25} \left( \frac{\omega}{\omega_c} \right)^{5/9} \right) \right] \frac{\omega}{\omega_c} \right\}$$

where

$$B = 0.14 \exp(23.e_y) e_y = \frac{S_y}{E'}$$

$$\frac{H_G}{S_y} = 2.84 \left[ 1 - \exp \left( -0.82 \left( \sqrt{\frac{\omega}{R}} \left( \frac{\omega}{1.9\omega_c} \right)^{B/2} \right)^{-0.7} \right) \right]$$

*Cubic Model*

$$\omega_c = \left( C_v \frac{\pi(1-\nu^2)Y}{2E^*} \right)^2 R, \quad \text{where } C = 1.234 + 1.256\nu$$

$$P_c = \frac{4E^* \sqrt{R}}{3} \omega_c^{3/2} \quad A_c = \pi R \omega_c$$

For  $1 \leq \omega/\omega_c \leq 110$

$$\frac{P}{P_c} = 0.2771 \left( \frac{\omega}{\omega_c} \right)^{3/2} + 2.1687 \left( \frac{\omega}{\omega_c} \right) - 2.1687 \left( \frac{\omega}{\omega_c} \right)^{1/2} + 0.7229$$

$$\frac{A}{A_c} = 0.0477 \left( \frac{\omega}{\omega_c} \right)^{3/2} + 1.4677 \left( \frac{\omega}{\omega_c} \right) - 1.0785 \left( \frac{\omega}{\omega_c} \right)^{1/2} + 0.5631$$

*BKE model*

$$\omega_c = \left( C_v \frac{\pi(1-\nu^2)Y}{2E^*} \right)^2 R, \quad \text{where } C = 1.234 + 1.256\nu$$

$$P_c = \frac{4E^* \sqrt{R}}{3} \omega_c^{3/2} \quad A_c = \pi R \omega_c$$

For  $\omega/\omega_c \geq 1$ ,

$$\frac{P}{P_c} = \left( \frac{\omega}{\omega_c} \right)^{3/2} \left[ 1 - e^{\left( \frac{-1}{1 - \left( \frac{\omega}{\omega_c} \right)^{0.174 + 0.08\nu}} \right)} \right] \quad \frac{A}{A_c} = \left( \frac{\omega}{\omega_c} \right) \left[ 1 + e^{\left( \frac{-1}{1 - \left( \frac{\omega}{\omega_c} \right)^{0.25 + 0.125\nu}} \right)} \right]$$



## References

1. Stachowiak A, Zwierycki W (2011) Tribocorrosion modeling of stainless steel in a sliding pair of pin on plate type. *Tribol Int* 44(10):1216–1224
2. Cao S, Guadalupe Maldonado S, Mischler S (2015) Tribocorrosion of passive metals in the mixed lubrication regime: theoretical model and application to metal on metal artificial hip joints. *Wear* 324–325:55–63
3. Cao S, Mischler S (2016) Assessment of a recent tribocorrosion model for wear of metal on metal hip joints: comparison between model predictions and simulator results. *Wear* 362–363:170–178
4. Cao S, Igual Munoz A, Mischler S (2017) Rationalizing the in vivo degradation of metal on metal artificial hip joints using tribocorrosion concepts. *Corrosion* 73(12):1510–1519
5. Guadalupe S, Gao S, Cantoni M, Chitty WJ, Falcand C, Mischler S (2017) Applicability of a recently proposed tribocorrosion model to CoCr alloys with different carbides content. *Wear* 376–377(Part A):203–211
6. Dalmanu A, Buch AR, Rovira A, Navarro-Laboulais J, Igual Munoz A (2018) Wear model for describing the time dependence of the material degradation mechanisms of the AISI 3161 in a NaCl solution. *Wear* 394–395:166–175
7. Vieira AC, Rocha LA, Papageorgiou N, Mischler S (2012) Mechanical and electro-chemical deterioration mechanisms in the tribocorrosion of Al alloys in NaCl and in NaNO<sub>3</sub> solutions. *Corros Sci* 54:26–35
8. Ghanbarzadeh A, Salehi FM, Bryant M, Neville A (2019) Modelling the evolution of electrochemical current in potentiostatic condition using an asperity scale model of tribocorrosion. *Biotribology* 17:19–29
9. Ghanbarzadeh A, Salehi FM, Bryant M, Neville A (2019) A new asperity-scale mechanistic model of tribocorrosive wear: synergistic effects of mechanical wear and corrosion. *ASME J Tribol* 141:021601
10. Greenwood JA, Williamson JBP (1966) Contact of nominally flat surfaces. *Proc R Soc Ser A* 295:300–319
11. Abbott EJ, Firestone FA (1933) Specifying surface quality - a method based on accurate measurement and comparison. *Mech Eng* 55:569–572
12. Chang WR, Etsion I, Bogy DB (1987) An elastic-plastic model for the contact of rough surfaces. *ASME J Tribol* 109:257–263
13. Zhao Y, Maietta DM, Chang L (2000) An asperity micro contact model incorporating the transition from elastic deformation to fully plastic flow. *ASME J Tribol* 122:86–93
14. Kogut L, Komvopoulos K (2004) Analysis of the spherical indentation cycle for elastic-perfectly solids. *J Mater Res* 19(12):3641–3653
15. Kogut L, Etsion I (2002) Elastic-plastic contact analysis of a sphere and a rigid flat". *ASME J Appl Mech* 69:657–662
16. Jackson RL, GreenGreen I (2005) A finite element study of elasto-plastic hemispherical contact against a rigid flat. *ASME J Tribol* 127:343–354
17. Jackson RL, Green I (2006) A statistical model of elasto-plastic asperity contact between rough surfaces. *Tribol Int* 39:906–914
18. Brizmer V, Kligerman Y, Etsion I (2006) The effect of contact conditions and material properties on the elasticity terminus of a spherical contact. *Int J Solids Struct* 43:5736–5749
19. Brizmer V, Zait Y, Kligerman Y, Etsion I (2006) The effect of contact conditions and material properties on elastic-plastic spherical contact. *Journal of Mechanics of Materials and Structures* 1(5):865–879
20. Shankar S, Mayuram MM (2008) A finite element based study on the elastic-plastic transition behavior in a hemisphere in contact with a rigid flat. *ASME J Tribol* 130(044502):1–6
21. Shankar S, Mayuram MM (2008) Effect of strain hardening in elastic-plastic transition behavior in a hemisphere in contact with a rigid flat. *Int J Solids Struct* 45:3009–3020
22. Megalingam A, Mayuram MM (2014) A comprehensive elastic-plastic single asperity contact model. *Tribol Trans* 57(2):324–335
23. Wang ZQ, Wang JF (2017) Model of a sphere-flat elastic-plastic adhesion contact. *ASME J Tribol* 139(4):041401
24. Wang ZQ (2013) A compact and easily accepted continuous model for the elastic-plastic contact of a sphere and a flat. *ASME J Appl Mech* 80(1):014506
25. Peng H, Liu Z, Huang F, Ma R (2013) A study of elastic-plastic contact of statistical rough surfaces. *Proc Inst Mech Eng Part J J Eng Tribol* 227(10):1076–1089
26. Ghaedina H, Pope SA, Jackson RL, Marghitu D (2016) A comprehensive study of the elasto-plastic contact of a sphere and a flat. *Tribol Int* 137(1):011403
27. Ghaednia H, Brake MDW, Berryhill M, Jackson RL (2019) Strain hardening from elastic-perfectly plastic to perfectly elastic flattening single asperity contact. *ASME J Tribol* 141:031402
28. Saha S, Xu Y, Jackson RL (2016) Perfectly elastic axisymmetric sinusoidal surface asperity contact. *ASME J Tribol* 138:031401
29. Ovcharenko A, Halperin, Verberne G, Etsion I (2007) In situ investigation of the contact area in elastic-plastic spherical contact during loading-unloading. *Tribol Lett* 25(2):153–160
30. Mc Cool JI (1986) Comparison of models for the contact of rough surfaces. *Wear* 107:37–60

**Publisher's Note** Springer Nature remains neutral with regard to jurisdictional claims in published maps and institutional affiliations.